Resubmitted to the International Journal of Solids and Structures in August 2014

Fracture analysis of an electrically conductive interface crack with a contact zone in a magnetoelectroelastic bimaterial system

P. Ma[a,b], R. K. L. Su[a,*] , W. J. Feng[b]

[a] *Department of Civil Engineering, The University of Hong Kong, PR China*

[b] *Department of Engineering Mechanics, Shijiazhuang Tiedao University, Shijiazhuang 050043, PR China*

Abstract

An electrically conductive interface crack with a contact zone in a magnetoelectroelastic (MEE) bimaterial system is considered. The bimaterial is polarized in the direction orthogonal to the crack faces and is loaded by remote tension and shear forces as well as electrical and magnetic fields parallel to the crack faces. It is assumed that the electrical field inside the crack faces is equal to zero and the magnetic quantities are continuous across the crack faces. Using special expressions of magnetoelectromechanical quantities via sectionally-analytic functions proposed in this paper, a combined Dirichlet-Riemann and Hilbert boundary value problem is formulated and solved analytically. Explicit analytical expressions for the characteristic mechanical, electrical and magnetic parameters are presented. A simple transcendental equation is derived for the determination of the contact zone length. Stress, electric field and magnetic field intensity factors and the contact zone length are found for various loading cases. A significant influence of the electric field on the contact zone length, stress and electric field intensity factors is observed. Magnetoelectrically permeable conditions in the crack region

[*] Corresponding author. Tel: +852 2859 2648; fax: +852 2559 5337
E-mail address: klsu@hku.hk (R.K.L. Su); wjfeng9999@126.com (W.J. Feng).

are also investigated and comparisons of different crack models are performed. Results presented in this paper should have potential applications to the design of multilayered magnetoelectroelastic (MEE) structures and devices.

Keywords: Electrically conductive interface crack; contact zone; magnetoelectroelastic material; field intensity factor

1. Introduction

As new multifunctional materials, magnetoelectroelastic (MEE) materials have found increasing applications in electronic technology, ultrasound technology, intelligence projects, as well as in other advanced smart structures, owing to their special magneto-electric coupling effect. However, MEE materials are usually brittle, possessing low fracture toughness and high imperfection sensitivity. These characteristics make the MEE devices susceptible to the formation of imperfections, such as cracks, during manufacture or service life and further lead to structural performance failure. Therefore, there has been tremendous interest in studying the fracture and failure behaviors of such materials (Zhou et al., 2004; Gao et al., 2004; Hu and Li, 2005; Feng et al., 2006; Feng and Su, 2006; Feng et al., 2007; Yong and Zhou, 2007; Wang et al., 2008; Li, 2001; Gao et al., 2003; Sih et al., 2003; Tian and Gabbert, 2005; Hu and Li, 2005; Zhou et al., 2007; Wang and Mai, 2007; Zhao and Fan, 2008; Singh et al., 2009; Hou et al., 2009; Chen, 2009; Zhong et al., 2009; Wang et al., 2010; Zhong and Zhang, 2010; Sladek et al., 2011; Sladek et al., 2012; Zhao et al., 2013; Han and Pan, 2013). In engineering practice, layered structures are very common. In such structures, interface delamination is probable, which will result in interfacial cracks. This is the main reason behind structural failure. In the past couple of decades, many researchers have studied the interface crack problems of MEE materials (Gao and Noda, 2004; Li and

Kardomateas, 2007; Zhao et al., 2008; Herrmann et al., 2010; Zhu et al., 2010; Feng et al., 2011; Ma et al., 2012).

On the other hand, electrically conductive cracks are very likely to form due to an extremely high local electric field inside the crack, since the dielectric permeability of the filling materials, such as air, is usually much less than that of MEE materials. In addition, electrode stratification or electrode-matrix debonding can often lead to the development of conductive cracks. When a conductive crack is loaded by an electrical and/or magnetic field parallel to the crack, electric charges in the conductive crack surfaces will rearrange themselves to develop an opposite field with the same magnitude, meaning that the electric field inside the conductive crack remains zero. Consequently, the charges in the upper and lower crack surfaces near the crack tip have the same sign. The phenomenon of these charges repelling each other has the effect of promoting crack propagation (Zhang et al., 2007). Therefore, the study of conductive cracks plays an important role in advancing our understanding of the failure behavior of MEE materials.

Moreover, for some combinations of magnetoelectromechanical loads, a crack between dissimilar MEE materials can develop a crack face contact zone. The contact zone may exert cardinal influence on magnetoelectromechanical fields in the whole crack region, especially at the crack tips. In such cases, applying the classic Griffith crack model (without considering the contact zone) would lead to a physically unrealistic overlapping of the crack faces and an introduction of a false stress concentration near the crack tip. The aim of the contact zone is to eliminate these crack face overlapping zones and to determine the true open crack formed and the corresponding fracture parameters. Recently, Herrmann et al. (2012) and Ma et al. (2012) for the first time extended the contact zone model to interface crack problems of MEE materials, whereupon the oscillating singularity on the crack tip is eliminated.

However, to our best knowledge, an electrically conductive crack in an MEE bimaterial system has not been studied yet, despite the possibility of the appearance of large contact zones for such cracks

under the action of electric and magnetic fields. This situation is significantly different from the aforementioned cases of the interface crack models proposed by Herrmann et al. (2010) and Ma et al. (2012), in which electrical and/or magnetic loads are perpendicular to the crack face and exert only a small influence on crack face contact. In the present study, we consider a new model, namely an electrically conductive crack with a frictionless contact zone in an MEE bimaterial system under the action of mechanical loading as well as the electrical and magnetic fields parallel to the crack faces. The expressions for contact zone length, stress intensity factors as well as electrical and magnetic field intensity factors are derived. Numerical results demonstrate that the contact zone indeed exists and can be found mathematically. Additionally, a significant influence of the electric field on the length of the contact zone and other fracture parameters is observed. These obtained results and/or conclusions could be of particular interest to the analysis and design of smart sensors/actuators composed of magnetoelectroelastic composite laminates.

2. Basic equations

The governing equations and general solutions for MEE half-spaces in a Cartesian coordinate system are consistent with those in Feng et al. (2011). Hence, for brevity, those equations will not be presented in this paper.

For the following analysis related to the conducting crack, it is convenient to introduce the vectors

$$\mathbf{C}=\left\{u_1',\ u_2',\ u_3',\ D_3,\ B_3\right\}^{\mathrm{T}},\ \mathbf{Y}=\left\{\sigma_{31},\ \sigma_{32},\ \sigma_{33},\ E_1,\ H_1\right\}^{\mathrm{T}}, \tag{1}$$

where u_1, u_2 and u_3 are the mechanical displacement components; E_1 and H_1 are the components of the electrical field and the magnetic field respectively; σ_{31}, σ_{32} and σ_{33} are the components of the stress; D_3 and B_3 are the components of the electrical displacement and the magnetic induction

respectively and the prime means the differentiation on x_1. Combined with the general solutions, these vectors can be written in the form (Loboda et al., 2014)

$$\mathbf{C} = \mathbf{M}\mathbf{f}'(z) + \bar{\mathbf{M}}\bar{\mathbf{f}}'(\bar{z}), \tag{2}$$

$$\mathbf{Y} = \mathbf{N}\mathbf{f}'(z) + \bar{\mathbf{N}}\bar{\mathbf{f}}'(\bar{z}), \tag{3}$$

where $\mathbf{f}(z) = \{\mathbf{f}_1(z_1), \mathbf{f}_2(z_2), \mathbf{f}_3(z_3), \mathbf{f}_4(z_4), \mathbf{f}_5(z_5)\}^{\mathrm{T}}$, $z_j = x_1 + p_j x_3 \ (j = 1,2,\cdots,5)$ and the matrices **M** and **N** are found by means of the reconstruction of the matrices **A** and **B** in Feng et al. (2011). They can be expressed as

$$\mathbf{M} = \{a_{1j}, a_{2j}, a_{3j}, b_{4j}, b_{5j}\}^{\mathrm{T}}, \ \mathbf{N} = \{b_{1j}, b_{2j}, b_{3j}, -a_{4j}, -a_{5j}\}^{\mathrm{T}}, \quad j = 1,2,...,5. \tag{4}$$

3. Statement of the problem

Figure 1 shows an electrically conducting crack located at $c \le x_1 \le b$, $x_3 = 0$ between two semi-infinite MEE half-spaces $x_3 > 0$ and $x_3 < 0$ with material properties defined by the following material constants $c_{ijks}^{(1)}$, $e_{iks}^{(1)}$, $h_{iks}^{(1)}$, $d_{is}^{(1)}$, $\alpha_{is}^{(1)}$, $\mu_{si}^{(1)}$ and $c_{ijks}^{(2)}$, $e_{iks}^{(2)}$, $h_{iks}^{(2)}$, $d_{is}^{(2)}$, $\alpha_{is}^{(2)}$, $\mu_{si}^{(2)}$, respectively. The half-spaces are assumed to be loaded at infinity with uniform stresses $\sigma_{33}^{(m)} = \sigma_0$, $\sigma_{31}^{(m)} = \tau_0$, electrical field $E_1^{(m)} = E_0$ and magnetic field $H_1^{(m)} = H_0$ (where m=1 stands for the upper domain and m=2 for the lower domain).

Furthermore, the crack surfaces are assumed to be traction-free for $x_1 \in (c,a) = L_1$ whereas they are in frictionless contact for $x_1 \in (a,b) = L_2$, and the position of Point a is arbitrarily chosen for the time being. It has been shown that the longer contact zone develops at the right crack tip for the shear stress at infinity $\tau_0 > 0$ if the lower material is softer than the upper one and it develops for $\tau_0 < 0$ in the opposite case (Loboda, 1998; Herrmann et al, 2001). Also it is revealed by Dundurs and Gautesen

(1998) and Kharun and Loboda (2003) that neglecting the left short contact zone, the oscillating singularity at the left crack tip will not significantly influence the stress and strain fields at the right crack tip. Therefore, in the present study only the contact zone at the right crack tip is considered. Certainly, a contact zone at the left crack-tip can be treated similarly.

Since the load and the displacement u_2 of the vector-function $(u_1, u_2, u_3, \varphi, \phi)$, in which φ and ϕ are the electrical potential and magnetic potential respectively, decouples in the (x_1, x_3)-plane from the components $(u_1, u_3, \varphi, \phi)$, in the following sections, our attention will be focused on the components $(u_1, u_3, \varphi, \phi)$ in a generalized plane strain condition.

Thus, for the present interface crack problem, the continuity and boundary conditions at the interface can be written in the following form:

$$\left[\tilde{\mathbf{C}}(x_1)\right] = \mathbf{0}, \quad \left[\tilde{\mathbf{Y}}(x_1)\right] = \mathbf{0}, \ x_1 \notin (c,b), \tag{5a}$$

$$\sigma_{13}^{(m)}(x_1,0) = 0, \ \sigma_{33}^{(m)}(x_1,0) = 0, \ E_1^{(m)}(x_1,0) = 0, \left[H_1(x_1)\right] = 0, \left[B_3(x_1)\right] = 0, \ x_1 \in L_1, \tag{5b}$$

$$\left[u_3(x_1)\right] = 0, \ \sigma_{13}^{(m)}(x_1,0) = 0, \left[\sigma_{33}(x_1)\right] = 0, \ E_1^{(m)}(x_1,0) = 0, \left[H_1(x_1)\right] = 0, \left[B_3(x_1)\right] = 0, \ x_1 \in L_2, \tag{5c}$$

where

$$\begin{aligned}\left[\tilde{\mathbf{C}}(x_1)\right] &= \left\{\left[u_1'(x_1)\right], \left[u_3'(x_1)\right], \left[D_3(x_1)\right], \left[B_3(x_1)\right]\right\}^{\mathrm{T}} \\ &= \left\{u_1'(x_1,0^+) - u_1'(x_1,0^-), \ u_3'(x_1,0^+) - u_3'(x_1,0^-), \ D_3(x_1,0^+) - D_3(x_1,0^-), \ B_3(x_1,0^+) - B_3(x_1,0^-)\right\}^{\mathrm{T}},\end{aligned} \tag{6a}$$

$$\begin{aligned}\left[\tilde{\mathbf{Y}}(x_1)\right] &= \left\{\left[\sigma_{31}(x_1)\right], \left[\sigma_{33}(x_1)\right], \left[E_1(x_1)\right], \left[H_1(x_1)\right]\right\}^{\mathrm{T}} \\ &= \left\{\sigma_{31}(x_1,0^+) - \sigma_{31}(x_1,0^-), \ \sigma_{33}(x_1,0^+) - \sigma_{33}(x_1,0^-), \ E_1(x_1,0^+) - E_1(x_1,0^-), \ H_1(x_1,0^+) - H_1(x_1,0^-)\right\}^{\mathrm{T}},\end{aligned} \tag{6b}$$

$$\left[u_3\left(x_1\right)\right]=u_3\left(x_1,0^+\right)-u_3\left(x_1,0^-\right). \tag{6c}$$

In Eqs. (5) and (6), square brackets mean the jump of the correspondent function through material interface, and the signs "+" and "-" denote the upper and lower parts of the interface. Additionally, it has been shown that for an electrically conductive crack the total electric charge on the crack faces may significantly influence the fracture parameter (Ru et al., 2000; Loboda and Mahnken, 2011; Knysh et al, 2012). In the present study, it is assumed that the total electric charge on crack faces is zero (Zhang et al., 2004; Gao et al., 2006), namely,

$$\int_c^b \left\{\left[D_3\left(x_1\right)\right]\right\} \mathrm{d}x_1 = 0. \tag{7}$$

4. The MEE solution

Similar to Loboda et al. (2014), from Eqs. (2), (3) and (5), the following expressions at the interface are obtained:

$$\left[\tilde{\mathbf{C}}\left(x_1\right)\right]=\mathbf{W}^+\left(x_1\right)-\mathbf{W}^-\left(x_1\right), \tag{8}$$

$$\tilde{\mathbf{Y}}^{(1)}\left(x_1,0\right)=\tilde{\mathbf{S}}\mathbf{W}^+\left(x_1\right)-\bar{\tilde{\mathbf{S}}}\mathbf{W}^-\left(x_1\right), \tag{9}$$

where $\mathbf{W}\left(z\right)=\left\{W_1\left(z\right),\ \ W_3\left(z\right),\ \ W_4\left(z\right),\ \ W_5\left(z\right)\right\}^{\mathrm{T}}$ is an introduced unknown vector function, and $\mathbf{W}^+\left(x_1\right)=\mathbf{W}\left(x_1+\mathrm{i}0\right),\ \ \mathbf{W}^-\left(x_1\right)=\mathbf{W}\left(x_1-\mathrm{i}0\right)$. The matrix $\tilde{\mathbf{S}}$ is reduced from the known matrix $\mathbf{S}$, defined as $\mathbf{S}=\mathbf{N}^{(1)}\mathbf{D}^{-1}$, $\mathbf{D}=\mathbf{M}^{(1)}-\bar{\mathbf{M}}^{(2)}\left(\bar{\mathbf{N}}^{(2)}\right)^{-1}\mathbf{N}^{(1)}$, by removing its second row and column. The matrix $\tilde{\mathbf{S}}$ has the following structure (Loboda et al., 2014):

$$\tilde{\mathbf{S}}=\begin{bmatrix}\tilde{S}_{11} & \tilde{S}_{13} & \tilde{S}_{14} & \tilde{S}_{15}\\ \tilde{S}_{31} & \tilde{S}_{33} & \tilde{S}_{34} & \tilde{S}_{35}\\ \tilde{S}_{41} & \tilde{S}_{43} & \tilde{S}_{44} & \tilde{S}_{45}\\ \tilde{S}_{51} & \tilde{S}_{53} & \tilde{S}_{54} & \tilde{S}_{55}\end{bmatrix}=\begin{bmatrix}\mathrm{i}s_{11} & s_{13} & \mathrm{i}s_{14} & \mathrm{i}s_{15}\\ s_{31} & \mathrm{i}s_{33} & s_{34} & s_{35}\\ \mathrm{i}s_{41} & s_{43} & \mathrm{i}s_{44} & \mathrm{i}s_{45}\\ \mathrm{i}s_{51} & s_{53} & \mathrm{i}s_{54} & \mathrm{i}s_{55}\end{bmatrix}, \tag{10}$$

where all s_{ij} are real and $s_{31}=-s_{13}$, $s_{41}=-s_{14}$, $s_{51}=-s_{15}$, $s_{43}=s_{34}$, $s_{53}=s_{35}$, $s_{54}=s_{45}$. Using the proposed expressions (8) and (9), many mixed mode problems for MEE bimaterials can be solved. These expressions are different from the traditional expressions of the magnetoelectromechanical quantities via sectionally analytic functions (Herrmann et al., 2010; Ma et al., 2012), because the third and fourth components of the vectors $\tilde{\mathbf{C}}$ and $\tilde{\mathbf{Y}}$ and the corresponding entries of the matrices **M** and **N** are permuted compared to the aforementioned expressions. It is important to note that the condition $\tilde{\mathbf{Y}}^{(1)}(x_1,0)=\tilde{\mathbf{Y}}^{(2)}(x_1,0)$ holds true for $x_1\in(-\infty,\infty)$. Therefore, Eqs. (8) and (9) are convenient for analyzing mixed problems provided that the components of the vector $\tilde{\mathbf{Y}}$ are continuous throughout the plane $x_3=0$. Moreover, by combining the boundary condition at infinity with Eqs. (8) and (9), it is easily found that $W_5^{\pm}(x_1)=W_{50}=\left\{\left(\mathbf{S}-\bar{\mathbf{S}}\right)^{-1}\tilde{\mathbf{Y}}_0\right\}_4$, where $\tilde{\mathbf{Y}}_0=\tilde{\mathbf{Y}}\big|_{x_1\to\infty}=\{\tau_0,\ \sigma_0,\ E_0,\ H_0\}^{\mathrm{T}}$.

Taking into account the fact that the magnetic quantities are continuous across the crack region, i.e., $\left[H_1(x_1)\right]=0$, $\left[B_3(x_1)\right]=0$ and introducing a row matrix $\mathbf{R}=\{R_1,\ R_3,\ R_4\}$ and considering a product $\mathbf{R}\hat{\mathbf{Y}}^{(1)}(x_1,0)$ with $\hat{\mathbf{Y}}^{(1)}(x_1,0)=\left\{\sigma_{31}^{(1)}(x_1,0),\ \sigma_{33}^{(1)}(x_1,0),\ E_1^{(1)}(x_1,0)\right\}^{\mathrm{T}}$, the following relations can be obtained from Eqs. (8) and (9):

$$\mathbf{R}\hat{\mathbf{Y}}^{(1)}(x_1,0)=\mathbf{F}^{+}(x_1)+\gamma\mathbf{F}^{-}(x_1)+\mathbf{Rh}, \tag{11}$$

where

$$\mathbf{F}(z)=\mathbf{T}\begin{Bmatrix}W_1(z)\\W_3(z)\\W_4(z)\end{Bmatrix},\ \mathbf{h}=\begin{Bmatrix}2\mathrm{i}s_{15}W_{50}\\0\\2\mathrm{i}s_{45}W_{50}\end{Bmatrix}, \tag{12a}$$

$$\mathbf{T}=\{T_1,\ T_3,\ T_4\}=\mathbf{R}\hat{\mathbf{S}},\ \hat{\mathbf{S}}=\begin{bmatrix}\mathrm{i}s_{11} & s_{13} & \mathrm{i}s_{14}\\ s_{31} & \mathrm{i}s_{33} & s_{34}\\ \mathrm{i}s_{41} & s_{43} & \mathrm{i}s_{44}\end{bmatrix}, \tag{12b}$$

and γ and $\mathbf{R}^{\mathrm{T}}$ are, respectively, the eigenvalues and eigenvectors of the system $\left(\gamma\hat{\mathbf{S}}^{\mathrm{T}}+\overline{\hat{\mathbf{S}}}^{\mathrm{T}}\right)\mathbf{R}^{\mathrm{T}}=0$. $\gamma_3=\gamma_1^{-1}$ and $\gamma_4=1$ hold true. The matrix $\mathbf{R}$ composed of eigenvectors $\mathbf{R}_j^{\mathrm{T}}$ has the following form:

$$\mathbf{R}=\begin{bmatrix} \mathrm{i}r_{11} & 1 & \mathrm{i}r_{14} \\ \mathrm{i}r_{31} & 1 & \mathrm{i}r_{34} \\ \mathrm{i}r_{41} & 0 & \mathrm{i} \end{bmatrix}, \tag{13}$$

where all r_{ij} are real and $r_{31}=-r_{11}$, $r_{34}=-r_{14}$ hold true. The components of the matrix $\mathbf{T}$ composed of line matrices $\mathbf{T}_j=\left\{T_{j1},\, T_{j3},\, T_{j4}\right\}=\mathbf{R}_j\mathbf{S}$ $(j=1,3,4)$ can be presented in the form $T_{j1}=t_{j1}$, $T_{j3}=\mathrm{i}t_{j3}$, $T_{j4}=t_{j4}$ where all t_{jk} $(j,k=1,3,4)$ are real and $t_{43}=0$.

It is worth mentioning that $F_j(z)=\mathbf{T}_j\mathbf{W}(z)$ $(j=1,3,4)$ have the same properties as $\mathbf{W}(z)$. For the boundary conditions (5), $F_j(z)$ are analytical in the whole plane except at the crack (c,b).

Taking into account the properties of the matrix $\mathbf{R}$ and $\mathbf{T}$ and Eq. (8), we have

$$r_{j3}\sigma_{33}^{(1)}(x_1,0)+\mathrm{i}r_{j1}\sigma_{13}^{(1)}(x_1,0)+\mathrm{i}r_{j4}E_1^{(1)}(x_1,0)=F_j^{+}(x_1)+\gamma_j F_j^{-}(x_1)+\eta_j, \tag{14}$$

$$t_{j1}\left[u_1'(x_1)\right]+\mathrm{i}t_{j3}\left[u_3'(x_1)\right]+t_{j4}\left[D_3(x_1)\right]=F_j^{+}(x_1)-F_j^{-}(x_1), \tag{15}$$

where $\eta_j=-2\left(r_{j1}s_{15}+r_{j4}s_{45}\right)W_{50}$, $r_{13}=r_{33}=r_{44}=1$ and $r_{43}=0$.

Considering that for $x_1\in L$, the relationships $F_j^{+}(x_1)=F_j^{-}(x_x)=F_j(x_x)$ holds true, one has

$$\left(1+\gamma_j\right)F_j(x_1)=\mathbf{R}_j\hat{\mathbf{Y}}^{(1)}(x_1,0)-\eta_j,\quad x_1\to\infty. \tag{16}$$

Using $\hat{\mathbf{Y}}^{(1)}(x_1,0)=\left[\tau_0,\, \sigma_0,\, E_0\right]^{\mathrm{T}}$ for $x_1\to\infty$, one can get

$$F_j(z)=\left(1+\gamma_j\right)^{-1}\left(r_{j3}\sigma_0+\mathrm{i}r_{j1}\tau_0+\mathrm{i}r_{j4}E_0-\eta_j\right),\quad x_1\to\infty. \tag{17}$$

By introducing new functions

$$\Theta_j(z)=F_j(z)+\left(1+\gamma_j\right)^{-1}\eta_j, \tag{18}$$

Eqs. (14), (15) and (17) can be written in the form

$$r_{j3}\sigma_{33}^{(1)}\left(x_1,0\right)+\mathrm{i}r_{j1}\sigma_{13}^{(1)}\left(x_1,0\right)+\mathrm{i}r_{j4}E_1^{(1)}\left(x_1,0\right)=\Theta_j^+\left(x_1\right)+\gamma_j\Theta_j^-\left(x_1\right), \tag{19}$$

$$t_{j1}\left[u_1'\left(x_1\right)\right]+\mathrm{i}t_{j3}\left[u_3'\left(x_1\right)\right]+t_{j4}\left[D_3\left(x_1\right)\right]=\Theta_j^+\left(x_1\right)-\Theta_j^-\left(x_1\right), \tag{20}$$

$$\Theta_j\left(z\right)\Big|_{z\to\infty}=\left(1+\gamma_j\right)^{-1}\left(r_{j3}\sigma_0+\mathrm{i}r_{j1}\tau_0+\mathrm{i}r_{j4}E_0\right). \tag{21}$$

By using boundary conditions (5b) and (5c) as well as Eqs. (19) and (20), we can obtain

$$\Theta_j^+\left(x_1\right)+\gamma_j\Theta_j^-\left(x_1\right)=0,\ \left(j=1,3,4\right),\quad x_1\in L_1, \tag{22}$$

$$\begin{cases}\mathrm{Im}\left\{\Theta_j^+\left(x_1\right)+\gamma_j\Theta_j^-\left(x_1\right)\right\}=0,\ \mathrm{Im}\left\{\Theta_j^+\left(x_1\right)-\Theta_j^-\left(x_1\right)\right\}=0,\ \left(j=1,3\right),\\ \Theta_4^+\left(x_1\right)+\Theta_4^-\left(x_1\right)=0,\end{cases}\quad x_1\in L_2. \tag{23}$$

It is remarked that the problems (22) are rather simple and can be solved by referring to Muskhelishvili (1963). However, this solution leads to the appearance of the oscillating singularity at crack tip and the overlapping of crack faces (Loboda et al., 2014). Eliminate these unrealistic phenomenon is the physical reason of introducing the contact zone.

Relations (22) and (23) for j=1, 3 lead to the following combined Dirichlet-Riemann boundary value problem:

$$\Theta_k^+\left(x_1\right)+\gamma_k\Theta_k^-\left(x_1\right)=0,\quad \left(k=1,3\right)\quad x_1\in L_1, \tag{24}$$

$$\mathrm{Im}\,\Theta_j^{\pm}\left(x_1\right)=0,\ \left(k=1,3\right)\quad x_1\in L_2. \tag{25}$$

While Eq. (22) for j=4 and $(23)_2$ lead to a Hilbert problem:

$$\Theta_4^+\left(x_1\right)+\Theta_4^-\left(x_1\right)=0,\quad x_1\in L_1\cup L_2, \tag{26}$$

with the condition at infinity

$$\Theta_j\left(z\right)\Big|_{z\to\infty}=\tilde{\sigma}_j-\mathrm{i}\,\tilde{\tau}_j,\quad j=1,3,4, \tag{27}$$

where $\tilde{\sigma}_j=r_{j3}\sigma_0/\vartheta_j$, $\tilde{\tau}_j=-\left(r_{j1}\tau_0+r_{j4}E_0\right)\big/\vartheta_j$, $\vartheta_j=1+\gamma_j$.

For the following analysis, it is sufficient to use the relation (24), (25) and (27) for j=1. The relations for j=3 are only required if some magnetoelectromechanical characteristics have to be found for the points situated outside the interface. Therefore, in the following section only the solution for j=1 will be considered.

An exact solution of the combined Dirichlet-Riemann boundary value problem (24), (25) and (27) for j=1 has been developed by Herrmann et al. (2010) and can be written as

$$\Theta_1(z) = P(z)X_1(z) + Q(z)X_2(z), \tag{28}$$

where $P(z)$, $Q(z)$, $X_1(z)$, $X_2(z)$ are given in Herrmann et al. (2010).

Substituting solution (28) into Eqs. (19) and (20), one can get the following expressions at the interface:

for $x_1 > b$:

$$r_{13}\sigma_{33}^{(1)}(x_1,0) + \mathrm{i}r_{11}\sigma_{13}^{(1)}(x_1,0) + \mathrm{i}r_{14}E_1^{(1)}(x_1,0) = \left\{\frac{Q(x_1)}{\sqrt{x_1-a}} + \frac{\mathrm{i}P(x_1)}{\sqrt{x_1-b}}\right\}\frac{\vartheta_1 \exp\{\mathrm{i}\varpi(x_1)\}}{\sqrt{x_1-c}}, \tag{29}$$

for $x_1 \in L_2$:

$$\begin{aligned}\sigma_{33}^{(1)}(x_1,0) = {} & \frac{\vartheta_1 P(x_1)}{\sqrt{(x_1-c)(b-x_1)}}\left\{\frac{1-\gamma_1}{1+\gamma_1}\cosh\varpi_0(x_1) + \sinh\varpi_0(x_1)\right\} \\ & + \frac{\vartheta_1 Q(x_1)}{\sqrt{(x_1-c)(x_1-a)}}\left\{\cosh\varpi_0(x_1) + \frac{1-\gamma_1}{1+\gamma_1}\sinh\varpi_0(x_1)\right\},\end{aligned} \tag{30a}$$

$$t_{11}\left[u_1'(x_1)\right] + t_{14}\left[D_3(x_1)\right] = \frac{2}{\sqrt{x_1-c}}\left\{\frac{P(x_1)}{\sqrt{b-x_1}}\cosh\varpi_0(x_1) + \frac{Q(x_1)}{\sqrt{x_1-a}}\sinh\varpi_0(x_1)\right\}, \tag{30b}$$

for $x_1 \in L_1$:

$$t_{11}\left[u_1'(x_1)\right] + \mathrm{i}t_{13}\left[u_3'(x_1)\right] + t_{14}\left[D_3(x_1)\right] = 2\sqrt{\alpha}\left\{\frac{P(x_1)}{\sqrt{b-x_1}} - \mathrm{i}\frac{Q(x_1)}{\sqrt{a-x_1}}\right\}\frac{\exp\{\mathrm{i}\varpi^*(x_1)\}}{\sqrt{x_1-c}}, \tag{31}$$

where $\alpha = (1+\gamma_1)^2 / 4\gamma_1$, and

$$\varpi(z) = 2\varepsilon \ln \frac{\sqrt{(b-a)(z-c)}}{\sqrt{l(z-a)} + \sqrt{(a-c)(z-b)}} \quad , \quad \varpi_0(x_1) = 2\varepsilon \tan^{-1} \sqrt{\frac{(a-c)(b-x_1)}{(b-c)(x_1-a)}}, \tag{32a}$$

$$\varpi^*(x_1) = 2\varepsilon \ln \frac{\sqrt{(b-a)(x_1-c)}}{\sqrt{l(a-x_1)} + \sqrt{(a-c)(b-x_1)}}, \quad \varepsilon = \frac{1}{2\pi} \ln \gamma_1 . \tag{32b}$$

The solution of the Hilbert problem (26) can be obtained by referring to Muskhelishvili (1963):

$$\Theta_4(z) = \frac{C_{04} + C_{14} z}{\sqrt{(z-c)(z-b)}} . \tag{33}$$

To determine the coefficients C_{04} and C_{14}, we use the condition at infinity (27) for j=4 and the condition for the total electric charge on crack faces, i.e., Eq.(7). By applying the Gaussian theorem to the contour that lies on the lower and upper faces of the crack, the singled-value conditions of displacement and the total electric charge in the crack region can be presented in the form (Knysh et al., 2012)

$$\int_c^b \left\{ \Theta_4^+(x_1) - \Theta_4^-(x_1) \right\} \mathrm{d}x_1 = 0 . \tag{34}$$

These give the following formula:

$$\Theta_4(z) = \frac{\mathrm{i}\Sigma_4}{2} \left(z - \frac{c+b}{2} \right) \frac{1}{\sqrt{(z-c)(z-b)}}, \tag{35}$$

where $\Sigma_4 = r_{41}\tau_0 + r_{44}E_0$.

It follows from Eq. (19) with an account $r_{43} = 0$ and Eq. (35) that

$$r_{41}\sigma_{13}^{(1)}(x_1, 0) + r_{44}E_1^{(1)}(x_1, 0) = \frac{2}{\mathrm{i}} \Theta_4(x_1) = \frac{\Sigma_4}{2} \left(x_1 - \frac{c+b}{2} \right) \frac{1}{\sqrt{(x_1-c)(x_1-b)}}, \; x_1 > b . \tag{36}$$

The imaginary part of Eq. (29) and Eq. (36) formulate a system of linear algebraic equations from

which the mechanical stress $\sigma_{13}^{(1)}(x_1,0)$ and the electric field $E_1^{(1)}(x_1,0)$ can be easily found for $x_1 > b$.

Using Eqs. (35) and (15) with *j*=4 and taking into account $t_{43} = 0$ one gets

$$t_{41}\left[u_1'(x_1)\right] + t_{44}\left[D_3(x_1)\right] = \left(x_1 - \frac{b+c}{2}\right)\frac{\Sigma_4}{\sqrt{(x_1-c)(b-x_1)}},\ x_1 \in L_1 \bigcup L_2. \tag{37}$$

From the system of linear algebraic equations composed of the real part of Eq. (31) and Eq. (37) for $x_1 \in L_1$ and of Eq. (30b) and Eqs. (37) for $x_1 \in L_2$, the expression for $\left[u_1'(x_1)\right]$ and $\left[D_3(x_1)\right]$ in the aforementioned intervals can be easily found.

By introducing the mechanical stress and electrical field intensity factors

$$k_1 = \lim_{x_1 \to a+0} \sqrt{2\pi(x_1-a)}\,\sigma_{33}(x_1,0), \tag{38a}$$

$$k_2 = \lim_{x_1 \to b+0} \sqrt{2\pi(x_1-b)}\,\sigma_{13}(x_1,0), \tag{38b}$$

$$k_E = \lim_{x_1 \to b+0} \sqrt{2\pi(x_1-a)}\,E_1(x_1,0), \tag{38c}$$

and using Eq. (30a) to determine k_1 and taking into account that $\varpi_0(a) = \ln\sqrt{\gamma_1}$, one has

$$k_1 = \sqrt{\frac{\pi l}{2\alpha}}\left(\xi_1 \cos\beta + \xi_2 \sin\beta\right). \tag{39}$$

where $\xi_1 = r_{13}\sqrt{1-\lambda}\,\sigma_0 + 2\varepsilon\Sigma_1$, $\xi_2 = \sqrt{1-\lambda}\,\Sigma_1 - 2\varepsilon r_{13}\sigma_0$, $\beta = \varepsilon \ln\dfrac{1-\sqrt{1-\lambda}}{1+\sqrt{1-\lambda}}$, $\lambda = (b-a)/l$, $l = b-c$.

By multiplying Eqs. (29) and (36) by $\sqrt{2\pi(x_1-b)}$ and considering $x_1 \to b+0$, the following system of linear algebraic equations are derived:

$$\begin{cases} r_{11}k_2 + r_{14}k_E = \sqrt{\dfrac{l}{2}}\,\omega, \\ r_{41}k_2 + r_{44}k_E = \sqrt{\dfrac{l}{2}}\,\Sigma_4, \end{cases} \tag{40}$$

where $\omega = \omega_1 \cos\beta - \omega_2 \sin\beta$, $\omega_1 = \Sigma_1 - 2\varepsilon\sqrt{1-\lambda}\sigma_0$, $\omega_2 = \sigma_0 + 2\varepsilon\sqrt{1-\lambda}\Sigma_1$, $\Sigma_1 = r_{11}\tau_0 + r_{14}E_0$.

Solving Eq. (40) gives the following expressions for k_2 and k_E:

$$k_2 = \sqrt{\frac{l}{2}}\frac{r_{44}\omega - r_{14}\Sigma_4}{r_{11}r_{44} - r_{14}r_{41}}, \quad k_E = \sqrt{\frac{l}{2}}\frac{r_{11}\Sigma_4 - r_{41}\omega}{r_{11}r_{44} - r_{14}r_{41}}. \tag{41}$$

Using Eq. (31) for $x_1 \to a - 0$ yields the following expression of $\left[u_3'(x_1)\right]$ via the stress intensity factor k_1:

$$\left[u_3'(x_1)\right] = -\frac{2\alpha}{t_{13}\vartheta_1\sqrt{2\pi(a - x_1)}}k_1. \tag{42}$$

Using Eqs. (30b) and (37) for $x_1 \to b - 0$ one gets

$$\begin{cases} t_{11}\left[u_1'(x_1)\right] + t_{14}\left[D_3(x_1)\right] = \dfrac{\omega}{\vartheta_1}\sqrt{\dfrac{l}{b - x_1}}, \\ t_{41}\left[u_1'(x_1)\right] + t_{44}\left[D_3(x_1)\right] = \dfrac{\Sigma_4}{2}\sqrt{\dfrac{l}{b - x_1}}, \end{cases} \quad x_1 \to b - 0. \tag{43}$$

From Eq. (43), the asymptotic expression for $\left[u_1'(x_1)\right]$ and $\left[D_3(x_1)\right]$ for $x_1 \to b - 0$ can be presented in the form

$$\left[u_1'(x_1, 0)\right]\Big|_{x_1 \to b-0} = \frac{1}{\sqrt{b - x_1}}\left(\Theta_{11}k_2 + \Theta_{14}k_E\right), \ \left[D_3(x_1)\right]\Big|_{x_1 \to b-0} = \frac{1}{\sqrt{b - x_1}}\left(\Theta_{41}k_2 + \Theta_{44}k_E\right). \tag{44}$$

where $\Theta_{11} = \left(2t_{44}r_{11} - \vartheta_1 t_{14}r_{41}\right)/\Delta$, $\Theta_{14} = \left(2t_{44}r_{14} - \vartheta_1 t_{14}r_{44}\right)/\Delta$, $\Theta_{41} = \left(\vartheta_1 t_{11}r_{41} - 2t_{41}r_{11}\right)/\Delta$, $\Theta_{44} = \left(\vartheta_1 t_{11}r_{44} - 2t_{41}r_{14}\right)/\Delta$, $\Delta = \sqrt{2}\vartheta_1\left(t_{11}t_{44} - t_{14}t_{41}\right)$.

Similarly, the field intensity factors associated with the crack opening displacement and electrical displacement jump across the crack near the crack tip are defined and easily derived as

$$k_{\mathrm{COD}}^3 = \lim_{x_1 \to a-0}\sqrt{\frac{\pi}{2(a - x_1)}}\left[u_3(x_1)\right] = \frac{2\alpha}{t_{13}\vartheta_1}k_1, \tag{45a}$$

$$k_{\mathrm{COD}}^{1}=\lim_{x_1\to b-0}\sqrt{\frac{\pi}{2\left(b-x_1\right)}}\left[u_1\left(x_1\right)\right]=-\sqrt{2\pi}\left(\Theta_{11}k_2+\Theta_{14}k_E\right), \tag{45b}$$

$$k_{\mathrm{D}}=\lim_{x_1\to b-0}\sqrt{\frac{\pi}{2}\left(b-x_1\right)}\left[D_3\left(x_1\right)\right]=\sqrt{\frac{\pi}{2}}\left(\Theta_{41}k_2+\Theta_{44}k_E\right). \tag{45c}$$

Considering that $\left[u_3'\left(x_1,0\right)\right]=W_3^+-W_3^-$, the first, third and fourth components of Eq. (9) can be written as

$$\begin{cases}\sigma_{13}^{(1)}\left(x_1,0\right)=\mathrm{i}s_{11}\left\{W_1^+\left(x_1\right)+W_1^-\left(x_1\right)\right\}+s_{13}\left[u_3'\left(x_1,0\right)\right]+\mathrm{i}s_{14}\left\{W_4^+\left(x_1\right)+W_4^-\left(x_1\right)\right\}+2\mathrm{i}s_{15}W_{50},\\ E_1^{(1)}\left(x_1,0\right)=\mathrm{i}s_{41}\left\{W_1^+\left(x_1\right)+W_1^-\left(x_1\right)\right\}+s_{43}\left[u_3'\left(x_1,0\right)\right]+\mathrm{i}s_{44}\left\{W_4^+\left(x_1\right)+W_4^-\left(x_1\right)\right\}+2\mathrm{i}s_{45}W_{50},\\ H_1^{(1)}\left(x_1,0\right)=\mathrm{i}s_{51}\left\{W_1^+\left(x_1\right)+W_1^-\left(x_1\right)\right\}+s_{53}\left[u_3'\left(x_1,0\right)\right]+\mathrm{i}s_{54}\left\{W_4^+\left(x_1\right)+W_4^-\left(x_1\right)\right\}+2\mathrm{i}s_{55}W_{50}.\end{cases} \tag{46}$$

By defining from the first and third components of Eq. (46) the expressions for $W_1^+\left(x_1\right)+W_1^-\left(x_1\right)$, and $W_4^+\left(x_1\right)+W_4^-\left(x_1\right)$, respectively, and substituting them into the third component of Eq. (46) we are led to the expression of $H_1^{(1)}\left(x_1,0\right)$ via $\sigma_{13}^{(1)}\left(x_1,0\right)$, $E_1^{(1)}\left(x_1,0\right)$ and $\left[u_3'\left(x_1,0\right)\right]$. On the basis of this obtained equation and taking into account $\sigma_{13}^{(1)}\left(x_1\right)=0$ and $\left[u_3'\left(x_1,0\right)\right]=0$ for $x_1\in L_2$, the following expression for magnetic field intensity factor has been defined and finally derived as follows:

$$k_H=\lim_{x_1\to b+0}\sqrt{2\pi\left(x_1-a\right)}H_1\left(x_1,0\right)=\frac{s_{11}s_{54}-s_{14}s_{51}}{s_{11}s_{44}-s_{14}s_{41}}k_E. \tag{47}$$

It is worthy to mention that the magnetic field intensity factor obtained from the present model is only dependent on the electrical field intensity factor, which is different from the previous contact zone model (Herrmann et al., 2010; Ma et al., 2012).

Additionally, it should be noted that the normal stress is singular in the left neighborhood of the crack tip and the corresponding intensity factor can be defined and derived as

$$k_1^b=\lim_{x_1\to b-0}\sqrt{2\pi\left(b-x_1\right)}\sigma_{33}\left(x_1,0\right)=\frac{1-\gamma_1}{1+\gamma_1}\sqrt{\pi}\left(r_{11}k_2+r_{14}k_E\right). \tag{48}$$

It is found that all field intensity factors for $x_1 \to b \pm 0$ in Eqs. (45), (47) and (48) are completely defined by k_1, k_2 and k_E.

5. Contact zone model

The solution of an interface crack problem, obtained in the previous chapter, is mathematically valid for any position of Point *a*. However, to preserve the physical sense of the obtained solutions, the following inequalities

$$\begin{cases} \sigma_{33}^{(1)}(x_1, 0) \le 0, & x_1 \in L_2, \\ [u_3] \ge 0, & x_1 \in L_1, \end{cases} \tag{49}$$

should be satisfied. In this case, the contact zone model in Comninous's (1977) sense takes place. The aforementioned position of Point *a* (or parameter λ) can be found from Eq. (39) by setting $k_1 = 0$ which leads to the following transcendental equation with respect to λ:

$$\tan\beta = \frac{\sqrt{1-\lambda}\,\sigma_0 + 2\varepsilon\Sigma_1}{2\varepsilon\sigma_0 - \sqrt{1-\lambda}\,\Sigma_1}. \tag{50}$$

To satisfy both inequalities (49) excluding the small zone of oscillation near the left crack tip, the maximum root of Eq. (50) from the interval (0, 1) should be taken.

The required solution $\lambda = \lambda_0$ of Eq. (50) can always be found numerically but if λ is small compared to 1, one can assume $\sqrt{1-\lambda} \approx 1$. This leads to the following asymptotic formula for $\bar{\lambda}_0 \approx \lambda_0$:

$$\bar{\lambda}_0 \approx 4\exp\left\{-\frac{1}{\varepsilon}\left[\tan^{-1}(2\varepsilon) - \tan^{-1}\left(\frac{\Sigma_1}{\sigma_0}\right) - \pi\left(n - \frac{1}{2}\right)\right]\right\}, \tag{51}$$

and the appropriate *n* should be taken.

It is seen from Eq. (38a) and Eq. (42) that, for $\lambda = \lambda_0$, the normal stress $\sigma_{33}^{(1)}(x_1, 0)$ is not singular at Point *a* and the crack closes smoothly at this point.

6. The crack faces free from electrodes

In this section, it is assumed that the electrodes are absent at the crack faces and the faces are free from mechanical, electrical and magnetic sources. In this case, the magnetoelectrically permeable and electrically impermeable and magnetically permeable conditions were considered by Herrmann et al. (2010) and by Ma et al. (2012), respectively, in which the electric displacement and/or magnetic induction was applied orthogonal to the crack faces. Since the contact zone model has never previously been considered for the electric and magnetic field parallel to the crack faces, and for the sake of comparison with the presented results, we consider the contact zone model for the crack faces to be free from electrodes. Taking into account that the derivation for magnetoelectrically permeable cracks and electrically impermeable and magnetically permeable cracks are similar, for simplicity the main attention will be paid to magnetoelectrically permeable cracks in this section.

For the problem depicted in Fig. 1, for the magnetoelectrically permeable crack assumption, the boundary conditions at the interface can be written in the form

$$\left[\tilde{\mathbf{L}}\left(x_1\right)\right]=\mathbf{0}, \quad \left[\tilde{\mathbf{Y}}\left(x_1\right)\right]=\mathbf{0}\,, \ x_1\notin\left(c,b\right), \tag{52a}$$

$$\sigma_{13}^{(m)}\left(x_1,0\right)=0,\ \sigma_{33}^{(m)}\left(x_1,0\right)=0,\left[E_1\left(x_1\right)\right]=0,\left[D_3\left(x_1\right)\right]=0,\left[H_1\left(x_1\right)\right]=0,\left[B_3\left(x_1\right)\right]=0\,,\ x_1\in L_1, \tag{52b}$$

$$\begin{cases}\left[u_3\left(x_1\right)\right]=0,\sigma_{13}^{(m)}\left(x_1,0\right)=0,\left[\sigma_{33}\left(x_1\right)\right]=0,\\ \left[E_1\left(x_1\right)\right]=0,\left[D_3\left(x_1\right)\right]=0,\left[H_1\left(x_1\right)\right]=0,\left[B_3\left(x_1\right)\right]=0,\end{cases} \quad x_1\in L_2\,. \tag{52c}$$

It follows from Eq. (51) that $\left[D_3\left(x_1\right)\right]=0$ and $\left[B_3\left(x_1\right)\right]=0$ for $x_1\in\left(-\infty,\infty\right)$. This relationship, together with Eq. (8), gives $W_4^+-W_4^-=0$ and $W_5^+-W_5^-=0$ for $x_1\in\left(-\infty,\infty\right)$ and means that W_4 and W_5 are analytical functions in the whole plane. Taking into account the constant value of magnetoelectromechanical quantities for $z\to\infty$, one has $W_4=W_{40}=const$ and $W_5=W_{50}=const$.

Moreover, by using Eq. (9) we have

$$W_4^{\pm}\left(x_1\right)=W_{40}=\left\{\left(\mathbf{S}-\overline{\mathbf{S}}\right)^{-1}\tilde{\mathbf{Y}}_0\right\}_3, W_5^{\pm}\left(x_1\right)=W_{50}=\left\{\left(\mathbf{S}-\overline{\mathbf{S}}\right)^{-1}\tilde{\mathbf{Y}}_0\right\}_4, \tag{53}$$

where $\tilde{\mathbf{Y}}_0=\tilde{\mathbf{Y}}\left(x_1,0\right)\big|_{x_1\to\infty}=\left\{\tau_0,\ \sigma_0,\ E_0,\ H_0\right\}^{\mathrm{T}}$.

Considering the form of matrix **S,** Eq. (9) can be written in the following form for $x_1\in\left(-\infty,\infty\right)$:

$$\begin{cases}\sigma_{13}^{(1)}\left(x_1,0\right)=\mathrm{i}s_{11}\left\{W_1^{+}\left(x_1\right)+W_1^{-}\left(x_1\right)\right\}+s_{13}\left\{W_3^{+}\left(x_1\right)-W_3^{-}\left(x_1\right)\right\}+2\mathrm{i}s_{14}W_{40}+2\mathrm{i}s_{15}W_{50},\\ \sigma_{33}^{(1)}\left(x_1,0\right)=s_{31}\left\{W_1^{+}\left(x_1\right)-W_1^{-}\left(x_1\right)\right\}+\mathrm{i}s_{33}\left\{W_3^{+}\left(x_1\right)+W_3^{-}\left(x_1\right)\right\},\\ E_1^{(1)}\left(x_1,0\right)=\mathrm{i}s_{41}\left\{W_1^{+}\left(x_1\right)+W_1^{-}\left(x_1\right)\right\}+s_{43}\left\{W_3^{+}\left(x_1\right)-W_3^{-}\left(x_1\right)\right\}+2\mathrm{i}s_{44}W_{40}+2\mathrm{i}s_{45}W_{50},\\ H_1^{(1)}\left(x_1,0\right)=\mathrm{i}s_{51}\left\{W_1^{+}\left(x_1\right)+W_1^{-}\left(x_1\right)\right\}+s_{53}\left\{W_3^{+}\left(x_1\right)-W_3^{-}\left(x_1\right)\right\}+2\mathrm{i}s_{54}W_{40}+2\mathrm{i}s_{55}W_{50}.\end{cases} \tag{54}$$

Combining the first and second relationships of Eqs. (54) leads to the following expression:

$$\sigma_{33}^{(1)}\left(x_1,0\right)+\mathrm{i}m_j\sigma_{13}^{(1)}\left(x_1,0\right)=t_j\left\{\Omega_j^{+}\left(x_1\right)+\gamma_j\Omega_j^{-}\left(x_1\right)\right\}-2m_j\left(s_{14}W_{40}+s_{15}W_{50}\right), \tag{55}$$

where

$$\Omega_j\left(z\right)=W_1\left(z\right)+\mathrm{i}\rho_jW_3\left(z\right),\ j=1,3, \tag{56}$$

and

$$\rho_j=\frac{s_{33}+m_js_{13}}{s_{31}-m_js_{11}},\ \gamma_j=-\frac{s_{31}+m_js_{11}}{s_{31}-m_js_{11}},\ m_{1,3}=\mp\sqrt{-\frac{s_{31}s_{33}}{s_{11}s_{13}}},\ j=1,3, \tag{57}$$

Eqs. (8) and (56) lead to the following expression for the derivations of the displacement jumps:

$$\left[u_1'\left(x_1\right)\right]+\mathrm{i}\rho_j\left[u_3'\left(x_1\right)\right]=\Omega_j^{+}\left(x_1\right)-\Omega_j^{-}\left(x_1\right),\ j=1,3, \tag{58}$$

and it is easily seen from Eqs. (52a) and (58) that the functions $\Omega_j\left(z\right)$ are analytical in the whole plane cut along $\left(c,b\right)$.

By performing a similar analysis to Herrmann et al. (2010), one can obtain the following transcendental equation for the determination of the contact zone length:

$$\tan\beta=\frac{\sqrt{1-\lambda}\sigma_0+2\varepsilon m_1\tau_0}{2\varepsilon\sigma_0-\sqrt{1-\lambda}m_1\tau_0}, \tag{59}$$

The shear stress can be found from the following formula:

$$k_2=-\frac{1}{m_1}\sqrt{\frac{\pi l}{2}}\left\{\left(\sigma_0\sin\beta-m_1\tau_0\cos\beta\right)+2\varepsilon\sqrt{1-\lambda}\left(\sigma_0\cos\beta+m_1\tau_0\sin\beta\right)\right\}. \tag{60}$$

It is worthy to mention that Eqs. (59) and (60) have the same form as seen in Herrmann et al. (2010), the only difference being that ε is calculated using the quantities related to matrix **S** in the present paper instead of matrix **G** in Herrmann et al. (2010).

After determination of the contact zone length from Eq. (59) the stress can be found by Eq. (55). Further, by use of Eq. (54) the electrical field can be found as

$$E_1^{(1)}\left(x_1,0\right)=\frac{s_{41}}{s_{11}}\left\{\sigma_{13}^{(1)}\left(x_1,0\right)-\tau_0\right\}+E_0,\ H_1^{(1)}\left(x_1,0\right)=\frac{s_{51}}{s_{11}}\left\{\sigma_{13}^{(1)}\left(x_1,0\right)-\tau_0\right\}+H_0,\ \ x_1\in L. \tag{61}$$

A detailed analysis of the contact zone model for an electrically impermeable and magnetically permeable crack was performed by Ma et al. (2012), and an insignificant difference in the contact zone length with respect to the present magnetoelectrically permeable crack was found for a pure mechanical loading case. Besides this, the influence of the applied electrical displacement orthogonal to the crack faces on the contact zone characteristics was found to be highly insignificant (Ma et al., 2010).

7. Numerical results and discussion

In this section, the numerical calculations are described. In all numerical procedures, σ_0 and τ_0 are, respectively, determined by σ and τ, where without loss of generality, $\sigma=\tau=4.2\times10^6\ \mathrm{N/m^2}$; and $\lambda_E=E_0e_{33}/\sigma$ is introduced to reflect the electrical load. Meanwhile, magnetic load H_0 is always set to zero. The interface crack between two dissimilar $CoFe_2O_4$-$BaTiO_3$ composites is considered. Material properties of the MEE materials as volume percentage (or volume fraction v_f) of $BaTiO_3$-

$CoFe_2O_4$ are listed in Table 1 (Annigeri et al., 2007; Feng et al., 2009). In what follows, material 1 and material 2 correspond to $CoFe_2O_4$-$BaTiO_3$ composites as v_f =0.2 and and v_f =0.4, respectively. A crack length of l=2 mm is assumed.

Firstly, the effects of shear load on the contact zone length, the Mode-II stress intensity factor and the electric field intensity factor are examined under only applied mechanical loads. Numerical results are plotted in Figs. 2-4, where $k_0 = \sqrt{0.5l}\sigma$ and $\lambda = (b-a)/l$. Fig. 2 shows that, for a fixed tension load, with the increasing of shear load, the contact zone length λ increases and finally tends to a constant. This is a new phenomenon for the electrically conductive crack problem although it has also been observed within the context of interface crack problems of both anisotropic bimaterial (Wang and Choi, 1983) and piezoelectric bimaterial (Herrmann and Loboda, 2000). For comparison, Fig. 2 simultaneously shows the corresponding contact zone length given by the corresponding formula in Ma et al. (2012) for the electrically impermeable and magnetically permeable interface crack model and the magnetoelectrically permeable crack model. The results shown in Fig. 2 demonstrate that there is a small difference in the contact zone length among the three models; however, the contact zone length finally reaches an identical constant of 0.3053 when the applied shear load is much larger than the tension load, which is equivalent to the case of pure shear load. Fig. 3 indicates that, as expected, the normalized Mode-II stress intensity factor k_2 increases with an increase of shear load. For comparison, the corresponding results calculated by the formula given in Ma et al. (2012) and the formula for magnetoelectrically permeable interface cracks are plotted simultaneously. It can be seen that the normalized Mode-II stress intensity factor k_2 obtained using the present model is less than that of the other two. This may be attributed to the variation of magnetoelectrical conditions throughout the crack region. Fig. 4 shows that, for a fixed tension load $\lambda_E = 0$, an increase in shear load will lead to an increase in the electric field intensity factor.

The relationship between the fracture parameters and the normalized electric load for different tension loads is presented in Figs. 5-7. The parameter of load combination λ_E varies from -3 to 3, i.e., the electric field E_0 from -3.15×10^6 V/m to 3.15×10^6 V/m. Fig. 5 shows that the contact zone length decreases rapidly as the electric field increases. This means that a large negative electric field may produce a large contact zone for the present model, which is consistent with the results given by Loboda et al. (2014) for conducting a crack model of piezoelectric bimaterial. In addition, Fig. 5 demonstrates that, as expected, increasing tension load leads to a rapid decrease in contact zone length. The results shown in Fig. 6 and Fig. 7 indicate that, for a fixed shear load, an increasing electric field causes increases in both the Mode-II stress intensity factor and electric field intensity factor. Additionally, an increase in tension load leads to an increase in the Mode-II stress intensity factor and a decrease in the electric field intensity factor.

The normalized displacement jump along the crack face and the normalized normal stress at the crack continuation for different tension loads are presented in Figs. 8 and 9, and these quantities for different electric fields are presented in Figs. 10 and 11. The origin of the coordinates is situated at the center of the crack region. Fig. 8 and Fig. 10 demonstrate that increasing tension load and the magnitude of negative electric field causes an increase in the maximum value of displacement jump. The results shown in Fig. 9 and Fig. 11 indicate that increasing tension load leads to an increase in normal stress at the crack continuation while increasing the magnitude of the negative electric field has the opposite effect. From Fig. 10 and Fig. 11, it can be seen that the electric field has a significant influence on crack opening displacement along the crack faces and the normal stress at the crack continuation. This is different from the case of the previous studied interface crack with contact zone, in which the influence of electrical displacement on the contact zone is not visible. Additionally, although the normal stress $\sigma_{33}(x_1,0)$ is not singular in the right neighborhood of point *b*, its value

remains very high in this region and perhaps can induce crack propagation. All these findings agree with the results given by Loboda et al. (2014) in their conducting of crack modeling of piezoelectric bimaterial. Fig. 8 and Fig. 10 also show that at $E_0 = 0$ the contact zone, which is equal to 2.056×10^{-3}, 1.230×10^{-5}, 6.648×10^{-8}, respectively, at σ_0/σ =1, 2, 3, is extremely small whilst, as a large negative electric field is applied, as shown in Fig. 5, the contact zone becomes much larger; for example at $E_0 = -5$, λ it is 0.02961 and at $E_0 = -10$, λ it is 0.06918. The obtained results confirm the strong influence of electric fields on the contact zone length and reveal that, for the combination of mechanical load, electric field and magnetic field, the classical open crack model induces an important error and, therefore, the contact zone model should be adopted. For comparison, the corresponding results for magnetoelectrically permeable cracks are also plotted simultaneously in Fig. 9 and Fig. 11. It can be seen that there is only a small difference in the obtained results between the electrically conductive crack model and the magnetoelectrically permeable crack under the pure mechanical loading case. However, whilst the electric field essentially influences the crack opening displacement along the crack face and the normal stress at crack continuation for electrically conductive cracks, it has no influence on magnetoelectrically permeable cracks. This phenomenon fully agrees with simple physical arguments because the crack does not disturb an electric field in magnetoelectrically permeable conditions.

8. Conclusions

A new model for interface cracks with a contact zone in an MEE bimaterial system under the action of a mixed-mode mechanical load as well as electric and magnetic fields parallel to the crack faces is considered. The interfacial crack is assumed to be an electrically conductive crack. Merging with the boundary conditions, a combination of the Dirichlet-Riemann boundary value problem and the

Hilbert problem is formulated. Using an exact analytical approach, the stress, electrical field and magnetic field intensity factors have been derived in a clear analytical form. The transcendental equations for the determination of real contact zone length have been obtained. Also, the case of magnetoelectrically permeable cracks is discussed. Finally, lots of numerical results are given graphically for the material combination of $BaTiO_3$–$CoFe_2O_4$ composites. From the theoretical and numerical results, the following conclusions can be drawn:

(i) In the present model, the magnetic field intensity factor is only dependent on the electrical field intensity factor and is independent of stress intensity factors, which differs from the results of previous crack models with contact zone.

(ii) The applied mechanical load and electrical field have important and different effects on the contact zone length. Among others, the contact zone length generally increases with an increase in shear load and decreases rapidly with an increase in tension load. Under a pure shear load, the contact zone length approaches a constant, which is mostly dependent on material constants. Additionally, a high negative electric field is likely to induce a large contact zone length.

(iii) The electrical field essentially influences the crack opening displacement along the crack faces and the normal stress at the crack continuation for electrically conductive cracks.

(iv) From the present model, the normal stress is not singular in the right neighborhood of Point *b* and it increases as the applied tension increases whilst decreasing as the magnitude of the negative electrical field increases.

Acknowledgement

Support from the National Natural Science Foundation of China (Grant Nos. 10772123 and 11072160), and the Training Program for Leading Talent in University Innovative Research Team in

Hebei Province (LJRC006) is acknowledged. The authors are also grateful to Professor T.Y. Zhang for his inspired advice on the proposed model in this paper.

References

Annigeri, A.R., Ganesan, N., Swarnamani, S., 2007. Free vibration behaviour of multiphase and layered magneto-electro-elastic beam. Journal of Sound and Vibration 299, 44-63.

Chen, X.H., 2009. Energy release rate and path-independent integral in dynamic fracture of magneto-electro-thermo-elastic solids. International Journal of Solids and Structures 46, 2706-2711.

Comninou, M.,1977. The interface crack. ASME Journal of Applied Mechanics 44, 631-636.

Dundurs, J., Gautesen, A.K., 1988. An opportunistic analysis of the interface crack. International Journal of Fracture 36, 151-159.

Feng, W.J., Li Y.S., Xu, Z.H., 2009. Transient response of an interfacial crack between dissimilar magnetoelectroelastic layers under magnetoelectromechanical impact loadings: Mode-I problem. International Journal of Solids and Structures 46, 3346-3356.

Feng, W.J., Ma, P., Pan, E., Liu, J.X., 2011. A magnetically impermeable and electrically permeable interface crack with a contact zone in a magnetoelectroelastic bimaterial under concentrated magnetoelectromechanical loads on the crack faces. Science China: Physics, Mechanics and Astronomy 54, 1666-1679.

Feng, W.J., Pan, E., Wang, X., 2007. Dynamic fracture analysis of a penny-shaped crack in a magnetoelectroelastic layer. International Journal of Solids and Structures 44, 7955-7974.

Feng, W.J., Su, R.K.L., 2006. Dynamic internal crack problem of a functionally graded magneto-electro-elastic strip. International Journal of Solids and Structures 43, 5196-5216.

Gao, C.F., Kessler, H., Balke, H., 2003. Crack problems in magnetoelectroelastic solids. Part I: Exact solution of a crack. International Journal of Engineering Science 41, 969-981.

Gao, C.F., Noda, N., 2004. Thermal-induced interfacial cracking of magnetoelectroelastic material. International Journal of Engineering Science 42, 1347-1360.

Gao, C.F., Noda, N., Zhang, T.Y., 2006. Dielectric breakdown model for a conductive crack and electrode in piezoelectric materials. International Journal of Engineering Science 44, 256-272.

Gao, C.F., Tong, P., Zhang, T.Y., 2004. Fracture mechanics for a mode III crack in a magnetoelectroelastic solid. International Journal of Solids and Structures 41, 6613-6629.

Han, X., Pan, E., 2013. Fields produced by three-dimensional dislocation loops in anisotropic magneto-electro-elastic materials. Mechanics of Materials 59, 110-125.

Herrmann, K.P., Loboda, V.V., 2000. Fracture mechanical assessment of electrically permeable interface cracks in piezoelectric bimaterials by consideration of various contact zone models. Archive of Applied Mechanics 70, 127-143.

Herrmann, K.P., Loboda, V.V., Govorukha, V.B., 2001. On contact zone models for an electrically impermeable interface crack in a piezoelectric biomaterial. International Journal of Fracture 111, 203-227.

Herrmann, K.P., Loboda, V.V., Khodanen, T.V., 2010. An interface crack with contact zones in a piezoelectric/piezomagnetic bimaterial. Archive of Applied Mechanics 80, 651-670.

Hou, P.F., Teng, G.H., Chen, H.R., 2009. Three-dimensional Green's function for a point heat source in two-phase transversely isotropic magneto-electro-thermo-elastic material. Mechanics of Materials 41, 329-338.

Hu, K.Q., Li, G.Q., 2005. Constant moving crack in a magnetoelectroelastic material under anti-plane shear loading. International Journal of Solids and Structures 42, 2823-2835.

Hu, K.Q., Li, G.Q., 2005. Electro-magneto-elastic analysis of a piezoelectromagnetic strip with a finite crack under longitudinal shear. Mechanics of Materials 37, 925-934.

Kharun, I.V., Loboda, V.V., 2003. A set of interface cracks with contact zones in combined tension-shear field. Acta Mechanica 166, 43-56.

Knysh, P., Loboda, V., Labesse-Jied, F., Lapusta, Y., 2012. An electrically charged crack in a piezoelectric material under remote electromechanical loading. International Journal of Fracture 175, 87-94.

Li, R., Kardomateas, G.A., 2007. The mixed mode I and II interface crack in piezoelectromagneto-elastic anisotropic bimaterials. ASME Journal of Applied Mechanics 74, 614-627.

Li, X.F., 2001. Dynamic analysis of a cracked magnetoelectroelastic medium under antiplane mechanical and inplane electric magnetic impacts. International Journal of Solids and Structures 42, 3185-3205.

Loboda, V.V., 1998. Analytical derivation and investigation of the interface crack models. International Journal of Solids and Structures 35, 4477-4489.

Loboda, V., Mahnken, R., 2011. An investigation of an electrode at the interface of a piezoelectric biomaterial space under remote electromechanical loading. Acta Mecanica 221, 327-339.

Loboda, V., Sheveleva, A., Lapusta, Y., 2014. An electrically conducting interface crack with a contact zone in a piezoelectric bimaterial. International Journal of Solids and Structures 51, 63-73.

Ma P., Feng W.J., Su, R.K.L., 2012. An electrically impermeable and magnetically permeable interface crack with a contact zone in a magnetoelectroelastic bimaterial under uniform magnetoelectromechanical loads. European Journal of Mechanics A-Solids 32, 41-51.

Muskhelishvili, N.I.,1963. Some Basic Problems of the Mathematical Theory of Elasticity. Noordhoff, Leyden.

Ru, C.Q., 2000. Exact solution for finite electrode layers embedded at the interface of two piezoelectric half-planes. Journal of the Mechanics and Physics of Solids 48, 693-708.

Sih, G.C., Jones, R., Song, Z.F., 2003. Piezomagnetic and piezoelectric poling effects on mode I and II crack initiation behavior of magnetoelectroelastic materials. Theoretical and Applied Fracture Mechanics 40, 161-186.

Singh, B.M., Rokne, J., Dhaliwal, R.S., 2009. Closed-form solutions for two anti-plane collinear cracks in a magnetoelectroelastic layer. European Journal of Mechanics A-Solids 28, 599-609.

Sladek, J., Sladek, V., Stanak, P., Zhang, C., Wünsche, M., 2011. An interaction integral method for computing fracture parameters in functionally graded magnetoelectroelastic composites. Computers Materials and Continua 23, 35-68.

Sladek, J., Sladek, V., Stanak, P., Zhang, C., Wünsche, M., 2012. Semi-permeable crack analysis in magnetoelectroelastic solids. Smart Materials and Structures 21, 025003.

Tian, W.Y., Gabbert, U., 2005. Macrocrack-microcrack interaction problem in magnetoelectroelastic solids. Mechanics of Materials 37, 565-592.

Wang, S.S., Choi, I.,1983. The interface crack between two dissimilar anisotropic composite materials. ASME Journal of Applied Mechanics 50, 169-178.

Wang, B.L., Han, J.C., Du, S.Y., 2010. Transient fracture of a layered magnetoelectroelastic medium. Mechanics of Materials 42, 354-364.

Wang, B.L., Mai, Y.W., 2007. Applicability of the crack-face electromagnetic boundary conditions for fracture of magnetoelectroelastic materials. International Journal of Solids and Structures 44, 387-398.

Wang, B.L., Sun, Y.G., Zhang, H.Y., 2008. Analysis of a penny-shaped crack in magnetoelectroelastic materials. Journal of Applied Physics 103, 083530-1-8.

Yong, H.D., Zhou, Y.H., 2007. Transient response of a cracked magnetoelectroelastic strip under anti-plane impact. International Journal of Solids and Structures 44, 705-717.

Zhang, T.Y., Liu, G., Wang, T., Tong, P., 2007. Application of the concepts of fracture mechanics to the failure of conductive cracks in piezoelectric ceramics. Engineering Fracture Mechanics 74, 1160-1173.

Zhang, T.Y., Zhao, M., Liu, G., 2004. Failure behavior and failure criterion of conductive cracks (deep notches) in piezoelectric ceramics I-the charge-free zone model. Acta Materialia 52, 2013-2024.

Zhao, M.H., Fan, C.Y., 2008. Strip electric-magnetic breakdown model in magnetoelectroelastic medium. Journal of the Mechanics and Physics of Solids 56, 3441-3458.

Zhao, M.H., Guo, Z.H., Fan, C.Y., Pan, E., 2013. Electric and magnetic polarization saturation and breakdown models for penny shaped cracks in 3D magnetoelectroelastic media. Journal of Solids and Structures 50, 1747-1754.

Zhao, M.H., Li, N., Fan, C.Y., Xu, G.T., 2008. Analysis method of planar interface cracks of arbitrary shape in three-dimensional transversely isotropic magnetoelectroelastic bimaterials. Journal of Solids and Structures 45, 1804-1824.

Zhong, X.C., Liu, F., Li, X.F., 2009. Transient response of a magnetoelectroelastic solid with two collinear dielectric cracks under impacts. Journal of Solids and Structures 46: 2950-2958.

Zhong X.C., Zhang, K.S., 2010. Dynamic analysis of a penny-shaped dielectric crack in a magnetoelectroelastic solid under impacts. European Journal of Mechanics A-Solids 29, 242-252.

Zhou, Z.G., Wang, B., Sun, Y.G., 2004. Two collinear interface cracks in magneto-electro-elastic composites. International Journal of Engineering Science 42, 1155-1167.

Zhou, Z.G., Zhang, P.W., Wu, L.Z., 2007. The closed form solution of a Mode-I crack in the piezoelectric/piezomagnetic materials. International Journal of Solids and Structures 44, 419-435.

Zhu, B.J., Shi, Y.L., Qin, T.Y., Sukop, M., Yu, S.H., Li, Y.B., 2010. Mixed-mode stress intensity factors of 3D interface crack in fully coupled electromagnetothermoelastic multiphase composites. International Journal of Solids and Structures 46, 2669-2679.

Figure and table captions

Fig. 1. An electrically conductive interface crack with frictionless contact zones under remote mixed mode mechanical load σ_0, τ_0, electrical field E_0 and magnetic field H_0

Fig. 2. Contact zone lengths versus the normalized applied shear load at $\sigma_0/\sigma = 1$ and $\lambda_E = 0$: (a) $10 \le \tau_0/\tau \le 100$; (b) $100 < \tau_0/\tau = 10^4$

Fig. 3. Normalized Mode-II stress intensity factor k_2/k_0 versus the normalized applied shear load at $\sigma_0/\sigma = 1$ and $\lambda_E = 0$

Fig. 4. Normalized electric field intensity factor k_E/k_0 versus the normalized applied shear load at $\sigma_0/\sigma = 1$ and $\lambda_E = 0$

Fig. 5. Contact zone lengths versus the applied electrical load λ_E for different tension loads at $\tau_0/\sigma = 50$

Fig. 6. Normalized Mode-II stress intensity factor k_2/k_0 versus the applied electrical load λ_E for different tension loads at $\tau_0/\sigma = 50$

Fig. 7. Normalized electric field intensity factor k_E/k_0 versus the applied electrical load λ_E for different tension loads at $\tau_0/\sigma = 50$

Fig. 8. Normalized crack opening displacement along the crack face for different tension loads at $\tau_0/\sigma = 50$ and $\lambda_E = 0$

Fig. 9. Normalized normal stress at the crack continuation for different tension loads at $\tau_0/\sigma = 50$ and $\lambda_E = 0$

Fig. 10. Normalized crack opening displacement along the crack face for different electric loads at $\sigma_0/\sigma = 1$ and $\tau_0/\sigma = 50$

Fig. 11. Normalized normal stress at the crack continuation for different electric loads at $\sigma_0/\sigma = 1$ and $\tau_0/\sigma = 50$

Table 1 Material properties of $BaTiO_3$-$CoFe_2O_4$ composites as a percentage (volume fraction v_f) (c_{ij} in 10^9 N/m^2, e_{ij} in C/m^2, ε_{ij} in 10^{-9}C/Vm, f_{ij} in N/Am, μ_{ij} in 10^{-4}Ns^2/ C^2, g_{ij} in 10^{-12}Ns/ VC), v_f=0.0 corresponding to $CoFe_2O_4$ and v_f=1.0 to $BaTiO_3$ (Annigeri et al., 2007; Feng et al., 2009)

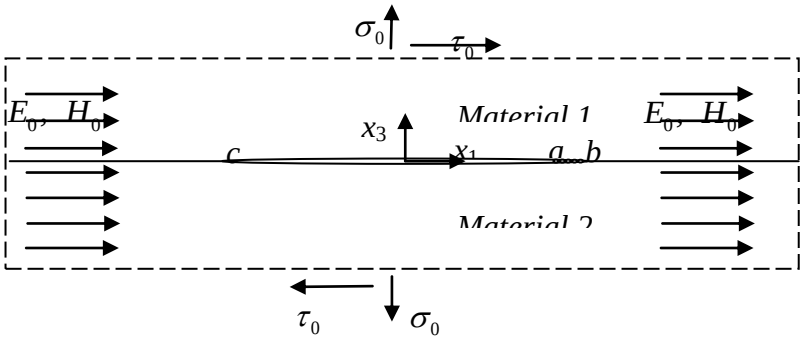

Fig. 1. An electrically conductive interface crack with frictionless contact zone under remote mixed mode mechanical load σ_0, τ_0, electrical field E_0 and magnetic field H_0

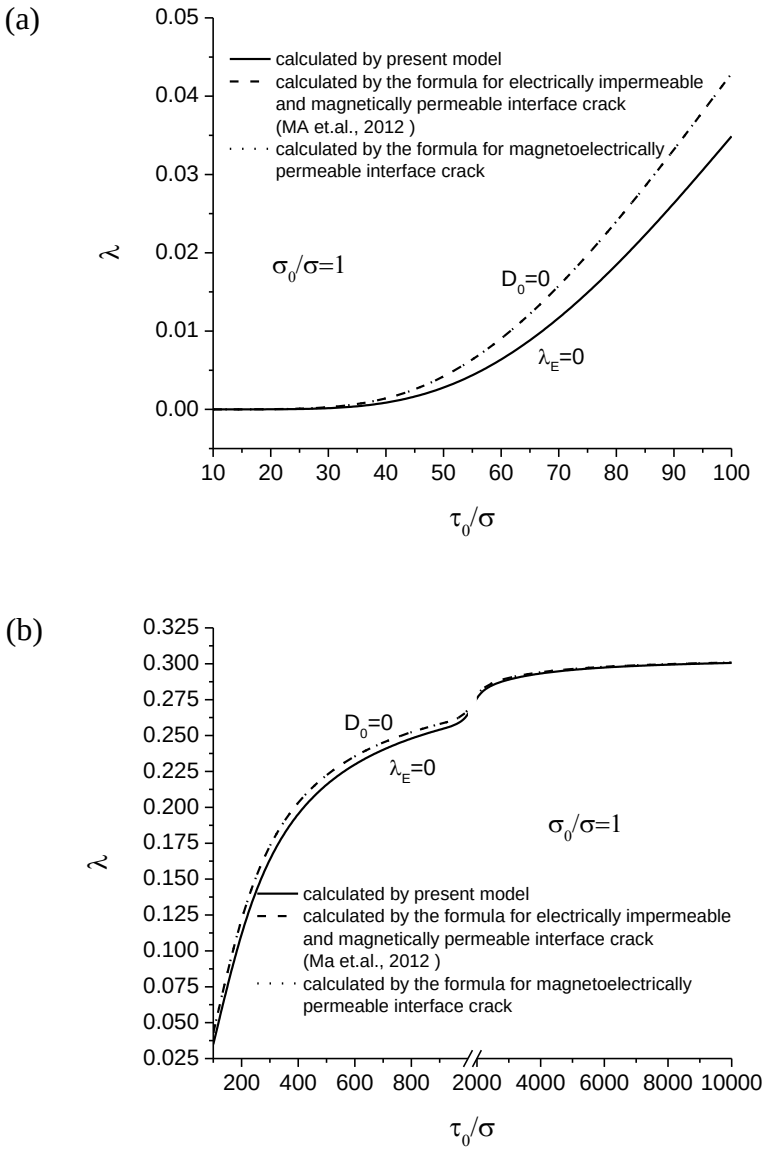

Fig. 2. Contact zone lengths versus the normalized applied shear load at $\sigma_0/\sigma=1$ and $\lambda_E=0$: (a) $10\le\tau_0/\tau\le100$; (b) $100<\tau_0/\tau=10^4$

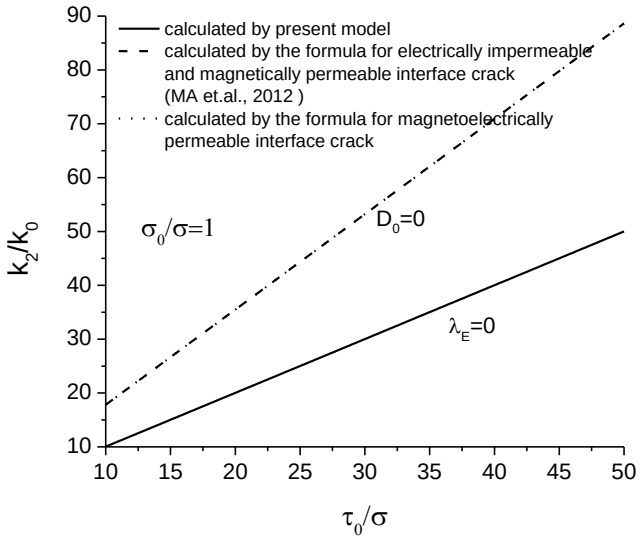

Fig. 3. Normalized Mode-II stress intensity factor k_2/k_0 versus the normalized applied shear load at $\sigma_0/\sigma=1$ and and $\lambda_E=0$

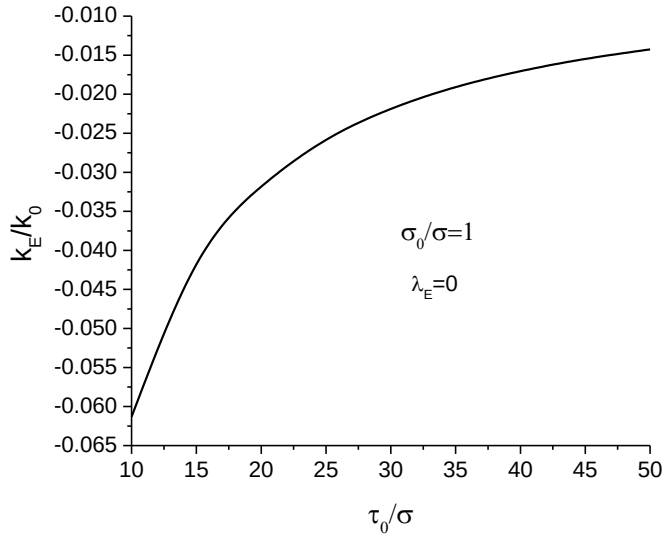

Fig. 4. Normalized electric field intensity factor k_E/k_0 versus the normalized applied shear load at $\sigma_0/\sigma = 1$ and $\lambda_E = 0$

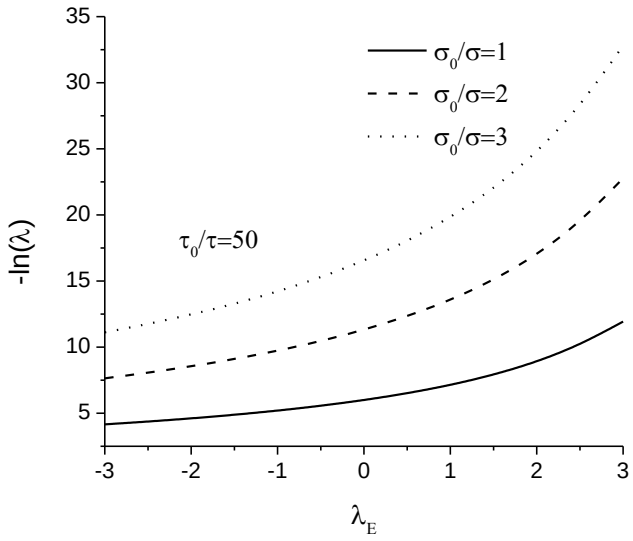

Fig. 5. Contact zone lengths versus the applied electrical load λ_E for different tension loads at $\tau_0/\sigma = 50$

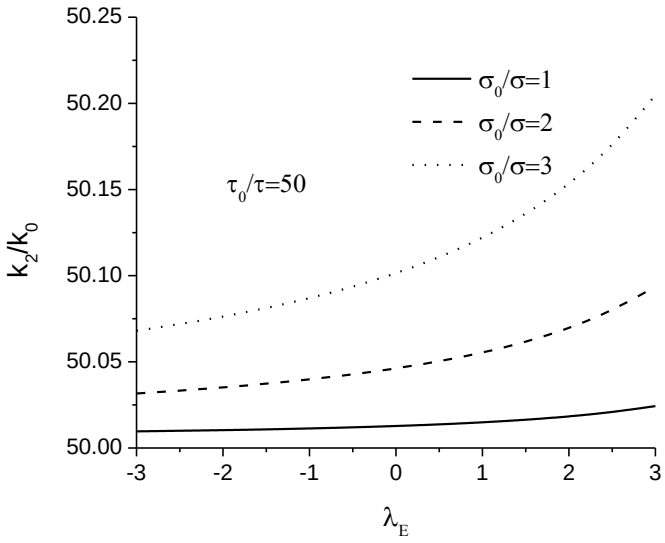

Fig. 6. Normalized Mode-II stress intensity stress k_2/k_0 versus the applied electrical load λ_E for different tension loads at $\tau_0/\sigma = 50$

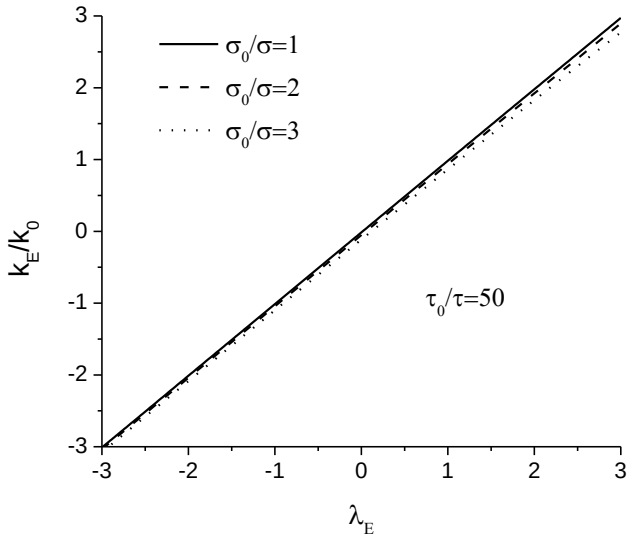

Fig. 7. Normalized electric field intensity factor k_E/k_0 versus the applied electrical load λ_E for different tension loads at $\tau_0/\sigma = 50$

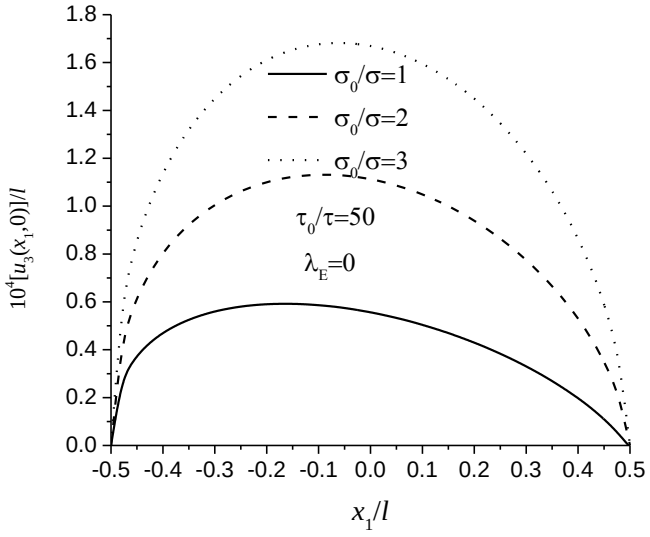

Fig. 8. Normalized crack opening displacement along the crack face for different tension loads at $\tau_0/\sigma = 50$ and $\lambda_E = 0$

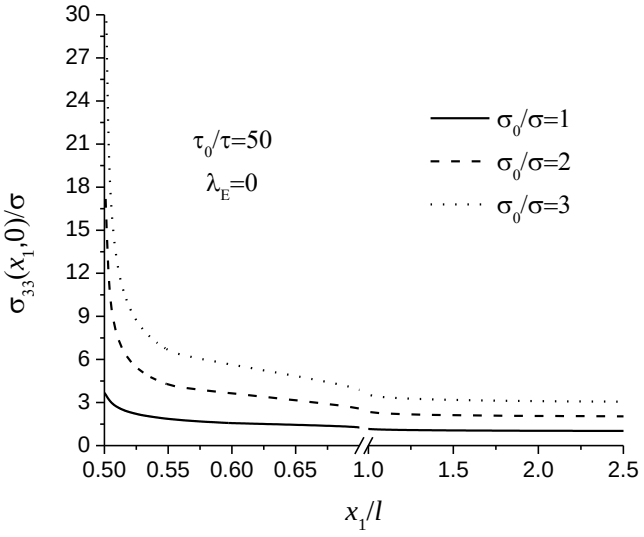

Fig. 9. Normalized normal stress at the crack continuation for different tension loads at $\tau_0/\sigma = 50$ and $\lambda_E = 0$

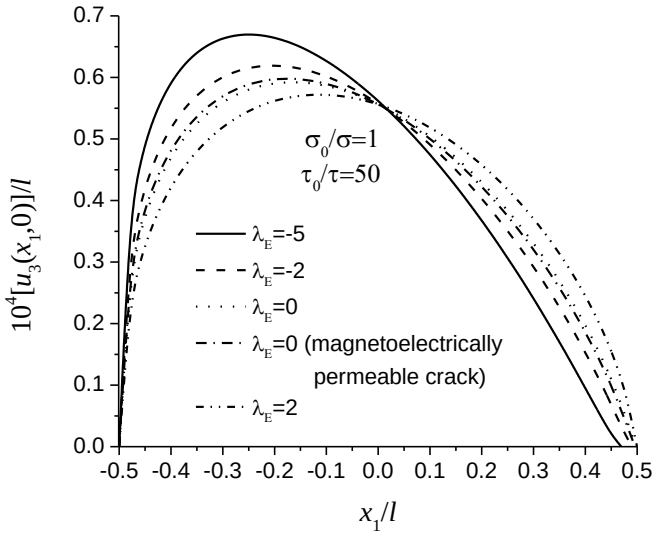

Fig. 10. Normalized crack opening displacement along the crack face for different electric loads at $\sigma_0/\sigma = 1$ and $\tau_0/\sigma = 50$

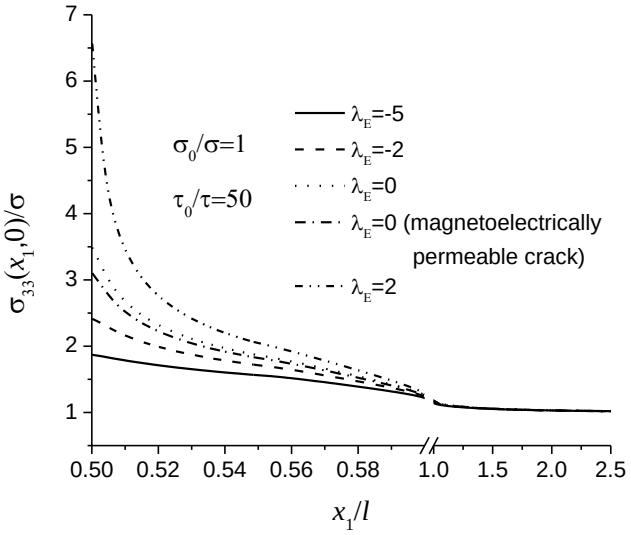

Fig. 11. Normalized normal stress at the crack continuation for different electric loads at $\sigma_0/\sigma=1$ and $\tau_0/\sigma=50$

Table 1

Material properties of $BaTiO_3$-$CoFe_2O_4$ composites as a percentage (volume fraction v_f) (c_{ij} in 10^9 N/m^2, e_{ij} in C/m^2, ε_{ij} in $10^{-9}C/Vm$, f_{ij} in N/Am, μ_{ij} in $10^{-4}Ns^2/C^2$, g_{ij} in $10^{-12}Ns/VC$), v_f=0.0 corresponding to $CoFe_2O_4$ and v_f=1.0 to $BaTiO_3$ (Annigeri et al., 2007; Feng et al., 2009)

	c_{11}	c_{12}	c_{13}	c_{33}	c_{44}	e_{15}	e_{31}	e_{33}	ε_{11}
v_f=0.2	250	146	145	240	45	0	-2	4	0.33
v_f=0.4	225	125	125	220	45	0	-3	7	0.8
	ε_{33}	μ_{11}	μ_{33}	f_{15}	f_{31}	f_{33}	g_{11}	g_{33}	
v_f=0.2	2.5	3.9	1.33	340	410	550	2.8	2000	
v_f=0.4	5.0	2.5	1.0	220	300	380	4.8	2750	